steady-state replenishment and loss are favorable.

References and Notes

(1) Haber, J.; Grzybowska, G. *J. Catal.* **1973**, *28*, 489. Haber, J. *Int. Chem. Eng.* **1975**, *15*, 21.
(2) Dadyburjor, D. B.; Jewur, S. S.; Ruckenstein, E. *Catal. Rev.—Sci. Eng.* **1979**, *19*, 293.
(3) Dadyburjor, D. B.; Ruckenstein, E. *J. Phys. Chem.* **1978**, *82*, 1563.
(4) Ruckenstein, E.; Dadyburjor, D. B. *AIChE J.* **1976**, *22*, 785.
(5) Dadyburjor, D. B.; Ruckenstein, E. *J. Catal.* **1980**, *63*, 383.
(6) Mars, P.; van Krevelen, D. W. *Chem. Eng. Sci. Suppl.* **1954**, *3*, 41.
(7) Yong, L. F.; Howe, R. F.; Keulks, G. W.; Hall, W. K. *J. Catal.* **1978**, *52*, 544.

Temperature Dependence of the Reaction $O(^3P) + OH(^2\Pi) \rightarrow O_2 + H$

R. S. Lewis† and R. T. Watson*

Jet Propulsion Laboratory, California Institute of Technology, Pasadena, California 91103

(Received: February 8, 1980; In Final Form: September 19, 1980)

The low-pressure discharge flow–resonance fluorescence technique has been utilized to study the kinetic behavior of ground-state atomic oxygen with hydroxyl radicals; pseudo-first-order conditions were used, $[O]_0 > [OH]_0$, in order to minimize complications caused by secondary kinetic processes. The reaction and the temperature dependence of the rate constant, expressed in units of cm^3 $molecule^{-1}$ s^{-1}, can be written in the following way: $O + OH \rightarrow H + O_2$; $\Delta H^\circ_{298} = -16.8$ kcal mol^{-1}; $k_1 = (2.01 \pm 0.18) \times 10^{-11} \exp((112 + 29)/T)$, 221–499 K; or $k_1 = (2.37^{+1.23}_{-0.81}) \times 10^{-10}\ T^{-(0.362\pm0.072)}$, 221–499 K. The experimental technique used affords the possibility of a small (6–10%) error being present in the measurements. This possibility is discussed in detail. The results are compared with previous measurements of k_1 and k_{-1} (using the thermodynamic equilibrium constant), and the role of this reaction in atmospheric chemistry is discussed.

Introduction

The reactions of HO are of great importance in atmospheric chemistry, and many of these reactions have been the subject of intense study. The HO radical plays a major role in the oxidation of SO_2, NO_2, CO, H_2S, hydrocarbons, halogenated alkanes, and alkanes in the troposphere and low stratosphere. The title reaction plays a major role in the chemistry of the upper stratosphere and mesosphere where O atoms become the dominant form of odd oxygen.[1] In this region, the O + OH reaction partially controls the OH/HO_2 ratio and in addition to the O + HO_2 reaction provides a sink for $O(^3P)$, thus partially controlling the odd oxygen concentration. In addition, the reaction is a major source of H atoms in the mesosphere.

There have been several absolute but somewhat indirect determinations of the $O(^3P)$ + OH rate constant, k_1, over a narrow temperature range, 228–340 K, using the low-pressure discharge flow technique.[2-8] Although the values obtained from these studies for k_1(298 K) cover a wide range, 0.5×10^{-11}–5.0×10^{-11} cm^3 $molecule^{-1}$ s^{-1}, the three lowest values[2,4,6] can be rejected on the basis of subsequent studies by the same authors,[5,8] resulting in values of k_1 ranging from 3×10^{-11} to 5×10^{-11} cm^3 $molecule^{-1}$ s^{-1}. There has also been one recent direct kinetic study using pseudo-first-order conditions with a combination discharge flow–flash photolysis–resonance fluorescence system at 298 K.[9] A value of 3.8×10^{-11} cm^3 $molecule^{-1}$ s^{-1} was determined for k_1 from this study which is in excellent agreement with the range of evaluated values[10-12] for k_1(298 K) of 3.8×10^{-11}–4.2×10^{-11} cm^3 $molecule^{-1}$ s^{-1} based on the more indirect studies. On the basis of the studies of Clyne[3] and Westenberg et al.,[8] where the reaction was studied over rather limited temperature ranges, it has been concluded in all recent evaluations[10-12] that the rate constant exhibits no temperature dependence. In addition to the absolute rate-constant studies, there has been one study where the $O(^3P)$ + OH rate constant was determined relative to the CO + OH rate constant at 425 K.[13] The result appears to be consistent with the absolute rate-constant determinations. In addition to the studies of the $O(^3P)$ + OH reaction, there have been numerous kinetic studies of the $H + O_2 \rightarrow OH + O$ reaction (reaction −1) between 700 and 2500 K,[14] the data of which have been the subject of several reviews and evaluations.[15,16] Unfortunately, combining the experimental values of k_1 and k_{-1} to determine the experimental equilibrium constant differs from the equilibrium constant determined from thermodynamic data by a factor of ~2. Consequently there is a need for an additional direct kinetic study of the O + OH reaction which will hopefully minimize the uncertainty in the absolute value of k_1 over a range of temperature so that it can be used in atmospheric-modeling calculations, and so the inconsistency in the values of k_1, k_{-1}, and K_{eq} (thermodynamic) can be explained.

In the present study, we have utilized the discharge flow–resonance fluorescence technique to measure directly the absolute rate and temperature dependence of reaction 1 over the temperature range 211–499 K. This study

$$O + OH \rightarrow O_2 + H \qquad (1)$$

represents the first direct study of this reaction over a wide range of temperature.

Experimental Section

The discharge flow–resonance fluorescence system used in this study has been described previously.[17] Therefore, only essential details will be given. A schematic of the system is shown in Figure 1. The flow tubes used in this study were constructed of quartz, mounted vertically and continuously evacuated by a 50-L s^{-1} rotary pump (Welch 1396) through two traps cooled to 77 K. The flow tubes consisted of three regions: (i) a resonance fluorescence

†NASA–NRC Resident Research Associate, 1976–1978.

0022-3654/80/2084-3495$01.00/0

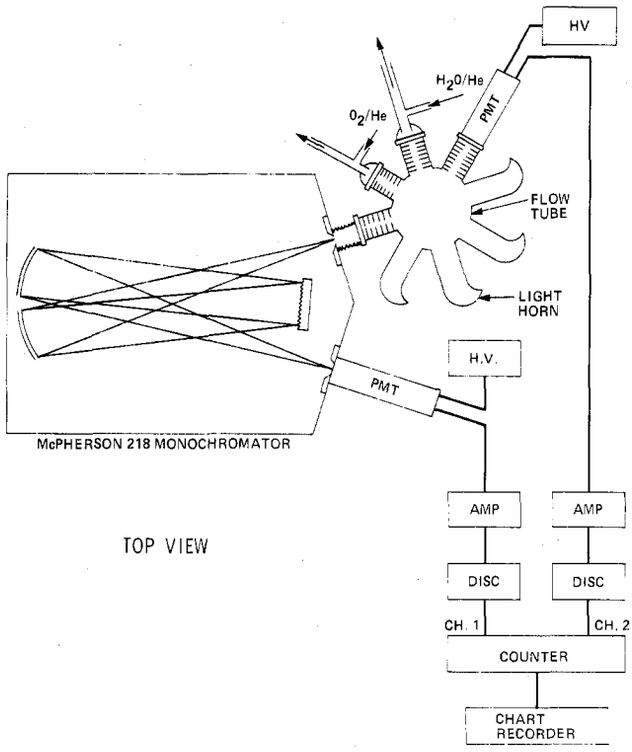

Figure 1. Schematic diagram of resonance-fluorescence apparatus.

detection region with two cells spaced 5 cm apart, (ii) a reaction zone of 70-cm length and 2.5-cm i.d. equipped with 12 fixed-position inlet jets and two side arms for atom production, and (iii) a section of 50-cm length and 5.0-cm i.d. above the reaction zone. At the top of this section was a side arm for oxygen-atom production and an inlet jet for NO_2 addition. Flow velocities of $\leq$4000 cm s^{-1} were attainable at room temperature in the reaction zone, but velocities under 1500 cm s^{-1} were used in order to minimize axial pressure gradients and to allow an adequate residence time in the flow system for the atomic-oxygen calibrations (discussed later). Two interchangeable tubes were used, one wrapped with Nichrome wire for the temperature range 298–499 K, with temperature control of ±5 K, and a double-walled tube whose temperature could be controlled to within ±0.5 K by circulating methanol through the outer jacket from a Haake constant-temperature bath and heat exchanger for the temperature range 211–298 K. The flow tubes were coated with dilute phosphoric acid and baked at 400 K under vacuum to minimize heterogeneous removal of OH. While this minimized γ(OH) from 220–500 K, it limited the maximum temperature to 500 K due to complications possibly associated with thermal decomposition of the phosphoric acid coating at higher temperatures.

As stated earlier there were two resonance-fluorescence scattering cells spaced 5 cm apart. The first of these was used to monitor the hydroxyl radical concentration via the $A^2\Sigma^+ \rightarrow X^2\Pi(0\text{–}0)$ transition, which is excited by a flowing water-saturated helium microwave plasma lamp operated at 2450 MHz and which is detected at right angles by a monochromator (McPherson 218) centered at 309.0 nm, a cooled photomultiplier (EMI 9659), and a photon counting system. The scattered light from the plasma lamp was minimized by using collimators in front of, and Wood's horns opposite, the resonance lamp and monochromator. The OH resonance-fluorescence signal was calibrated as part of every kinetic experiment by generating known concentrations of OH from the reaction of NO_2 with an excess concentration of hydrogen atoms (eq 2). The fluorescence signal was typically $\sim 10^3$ Hz for a

$$H + NO_2 \rightarrow OH + NO \quad (2)$$

$$k_2 = 1.41 \times 10^{-10} \text{ cm}^3 \text{ molecule}^{-1} \text{ s}^{-1} \text{ (ref 18)}$$

hydroxyl radical concentration of 10^{11} cm^{-3}, in contrast to a background signal (scattered light plus photomultiplier dark noise) of $\sim 10^2$ Hz. Consequently a detection limit of $\sim 10^9$ cm^{-3} ($S/N = 1$) was obtainable when the normal experimental procedure of averaging six 10-s counting periods was used. The second scattering cell was used to monitor the concentration of $O(^3P)$ atoms via the unresolved $(2p^33s)^3S_1\text{–}(2p^4)\ ^3P_{0,1,2}$ multiplet from 130.2 to 130.6 nm. The $O(^3P)$ atomic resonance fluorescence was excited by a flowing O_2/He microwave plasma lamp with a CaF_2 window and detected at right angles by a solar blind photomultiplier (EMR 542G). A second CaF_2 window was used as a filter above the photomultiplier so that no 121.6-nm Lyman-α radiation could be detected even in the presence of high concentrations of atomic hydrogen ($\sim 10^{13}$ cm^{-3}) in the flow tube. Atomic oxygen was normally produced by dissociating a small amount of molecular oxygen mixed with $\sim$10% of the total helium flow in a microwave discharge bypass system. This bypass technique minimized the level of atomic impurities produced in the discharge region (atomic hydrogen produced as an impurity would affect the calibration for atomic-oxygen concentrations) and allowed greater control of atomic-oxygen concentrations. A few kinetic runs were performed at 298 K by reacting atomic nitrogen with nitric oxide (eq 3) as the source of atomic oxygen. An excess of NO was

$$N + NO \rightarrow N_2 + O(^3P) \quad (3)$$

$$k_3 = 3.4 \times 10^{-11} \text{ cm}^3 \text{ molecule}^{-1} \text{ s}^{-1} \text{ (ref 12)}$$

added to the flow of atomic nitrogen which was produced by dissociating N_2 in a microwave discharge. Atomic-oxygen concentrations were determined by titrating the $O(^3P)$ atoms with NO_2 (eq 4) after each kinetic run using ex-

$$O(^3P) + NO_2 \rightarrow NO + O_2 \quad (4)$$

$$k_4 = 9.3 \times 10^{-12} \text{ cm}^3 \text{ molecule}^{-1} \text{ s}^{-1} \text{ (ref 12)}$$

perimental conditions (i.e., flow velocity and total pressure) identical with those used in the kinetic run. The $O(^3P)$ fluorescence signal was typically $\sim 10^5$ Hz for an atomic-oxygen concentration of 10^{12} cm^{-3}, in contrast to a background signal of 2×10^2 Hz which was again minimized by using collimators and Wood's horns. Consequently the detection limit for $O(^3P)$ was $<10^9$ cm^{-3} ($S/N = 1$) using the normal counting procedure.

A typical experiment was carried out in the following manner. First, OH was produced by adding NO_2 ($\sim 1.5 \times 10^{11}$ cm^{-3}) to a flow of H atoms ($\sim 1.5 \times 10^{13}$ cm^{-3}) at each of the inlet jets. This gives a value of $[OH]_t$ at each jet, and a measure of k_w, the first-order rate constant for heterogeneous removal of OH. The procedure is then repeated in the presence of atomic oxygen ($1 \times 10^{12}\text{–}7 \times 10^{12}$ cm^{-3}), thus generating a value of $[OH]_t^*$ for each jet. The atomic hydrogen and NO_2 flows were then stopped, and the $O(^3P)$ concentration was determined via an NO_2 titration under experimental conditions.

Reagent flow rates and pressure were determined by using calibrated mass flow meters (Hasting-Raydist) and MKS Baratron pressure sensors, respectively. The gases used in this study were helium, hydrogen (both Linde Ultra High Purity), and oxygen (Matheson Research Grade). These gases were used with no further purification. NO_2 was purified by several freeze–pump–thaw cycles until no

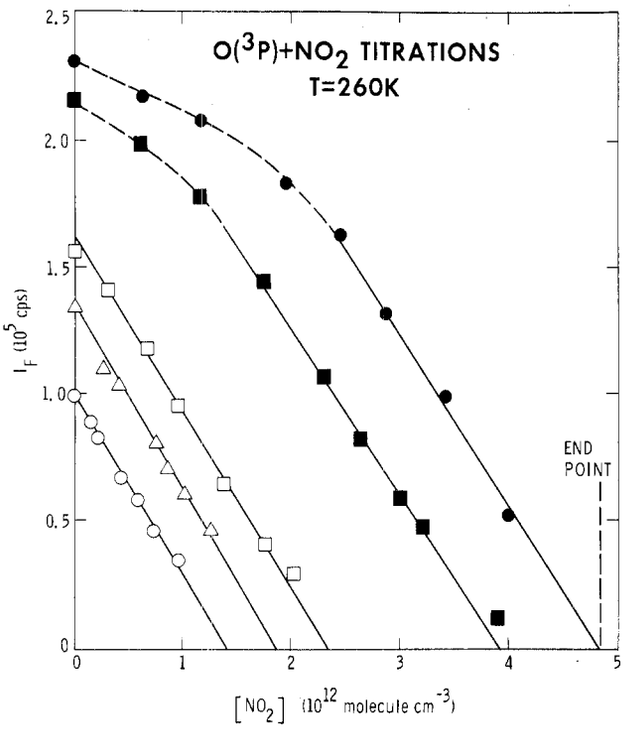

Figure 2. Determination of atomic-oxygen concentration using the O + NO_2 reaction. Plots of oxygen-atom resonance-fluorescence intensity (I_F) as a function of added NO_2 concentration at 260 K.

blue coloration due to NO could be seen in the frozen solid N_2O_4.

Results

Determination of [O, ^3P]. Atomic oxygen was produced at the top of the flow tube. NO_2 could be added to the flow of oxygen atoms via an inlet jet which typically allowed a reaction time of ~0.25 s. However, the time required for >95% removal of $O(^3P)$ by NO_2 under pure second-order conditions (where $[O]_0 = [NO_2]_0$) is greater than 0.25 s, e.g., for [O, $^3P]_0 = 3 \times 10^{12}$ cm^{-3}, $\tau_{0.95} = 0.68$ s. Consequently the approach taken in this study was not to determine [O,(^3P)] by an end-point titration under second-order conditions, but to monitor the oxygen-atom fluorescence signal as a function of added [NO_2] and to extrapolate the linear portion (where I_F is assumed to vary linearly with [O,(^3P)]) of the plot to the [NO_2] axis where the fluorescence signal was indistinguishable from the background signal. The intercept was taken to be equal to the titration end point where $[O]_0 = [NO_2]_0$. Figure 2 shows a set of oxygen-atom titration plots taken at 260 K (these plots were all taken on the same day where the plasma lamp conditions, i.e., sensitivity, remained constant). This approach should allow the determination of the $O(^3P)$ concentration to be made to within an accuracy of ~10% for the complete range used in this study (1.3×10^{12}–7.3×10^{12} cm^{-3}). The nonlinearity observed in some of the plots shown in Figure 2 is due to self-reversal. This observation is expected at these concentrations for an atom such as $O(^3P)$ with a high oscillator strength, $f \simeq 0.031$.[19] The onset of nonlinearity is dependent upon the plasma lamp conditions, i.e., the extent of self-reversal, the geometry and optical depth of the scattering volume, and the f values of the transitions being monitored. The onset of nonlinearity between I_F and [O,^3P] in this system occurred at $\sim 2 \times 10^{12}$–3×10^{12} cm^{-3}, quite similar to that reported in previous studies[20] (e.g., $\sim 1 \times 10^{12}$ cm^{-3}). The heterogeneous removal of $O(^3P)$ along the length of the flow tube was shown to be negligible, <5% ($\gamma < 5 \times 10^{-5}$), by adding

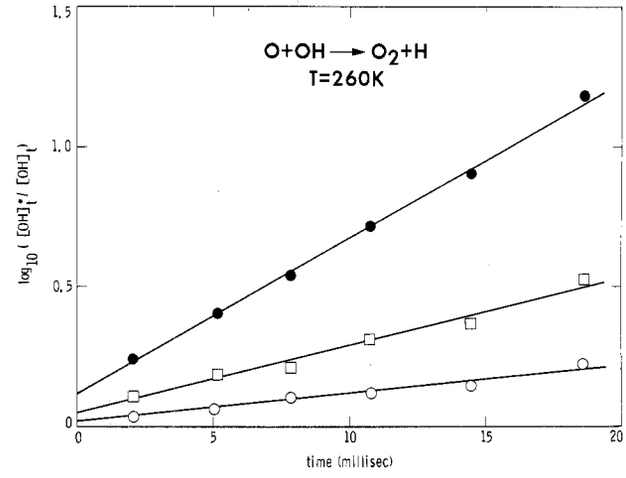

Figure 3. The reaction $O(^3P) + OH \rightarrow O_2 + H$. Typical first-order plots for [OH] in the presence of various excess concentrations of $O(^3P)$ at 260 K: (○) $[O]_0 = 1.43 \times 10^{12}$ cm^{-3}, $[OH]_0 = 1.2 \times 10^{11}$ cm^{-3}; (□) $[O]_0 = 2.29 \times 10^{12}$ cm^{-3}, $[OH]_0 = 4.0 \times 10^{11}$ cm^{-3}; (●) $[O]_0 = 4.62 \times 10^{12}$ cm^{-3}, $[OH]_0 = 1.9 \times 10^{11}$ cm^{-3}.

NO to an excess concentration of atomic nitrogen at several different inlet jets and monitoring the intensity of the $O(^3P)$ resonance fluorescence. This is consistent with previous studies which have reported values of $\gamma(O(^3P))$ of 2×10^{-5}–12×10^{-5} (unpoisoned Pyrex)[21] and 1×10^{-7}–30×10^{-7} (H_3PO_4-coated Pyrex).[21]

Determination of k_1. The kinetic behavior of ground-state atomic oxygen with $OH(^2\Pi)$ was studied from 221 to 499 K by using pseudo-first-order conditions, $[O]_0 > [OH]_0$ ($[O]_0 = 1.3 \times 10^{12}$–$7.3 \times 10^{12}$ cm^{-3}; $[OH]_0 = 0.9 \times 10^{11}$–$4.2 \times 10^{11}$ cm^{-3}; giving a range of initial stoichiometry of 5.5–33, with a typical value of ~14). The reaction scheme can be written as follows:

$$H + NO_2 \rightarrow OH + NO \quad (2)$$

$$O + OH \rightarrow O_2 + H \quad (1)$$

$$OH + \text{wall} \rightarrow \text{products} \quad (w)$$

The following equations describe the hydroxyl radical concentration as a function of time:

$$[OH]_t(\text{absence of } O(^3P)) = \frac{k_2'[NO_2]_0}{k_w - k_2'}\{e^{-k_2't} - e^{-k_wt}\} \quad (I)$$

$$[OH]_t^*(\text{presence of } O(^3P)) = \frac{k_2'[NO_2]_0}{k_1' + k_w^* - k_2'}\{e^{-k_2't} - e^{-(k_1' + k_w^*)t}\} \quad (II)$$

where $k_2' = k_2[H]_0$; $k_1' = k_1[O]_0$; k_w = first-order heterogeneous rate constant for OH removal in the absence of $O(^3P)$; k_w^* = first-order heterogeneous rate constant for OH removal in the presence of $O(^3P)$. Combining eq I and II yields

$$\frac{[OH]_t}{[OH]_t^*} = \frac{k_1' + k_w^* - k_2'}{k_w - k_2'}\left\{\frac{e^{-k_2't} - e^{-k_wt}}{e^{-k_2't} - e^{-(k_1' + k_w^*)t}}\right\} \quad (III)$$

In all experiments, OH was formed by reaction 2 on a time scale ($\tau_{1/2} < 0.5$ ms) at least 20 times faster than its loss ($\tau_{1/2} > 10$ ms), thus simplifying the data analysis considerably. From eq III, and under the experimental conditions used in this study, it can be shown that

$$\ln([OH]_t/[OH]_t^*) = \{k_1' - (k_w - k_w^*)\}t \quad (IV)$$

A typical decay plot is shown in Figure 3. The decay of [OH] is clearly exponential over a factor of 20, verifying that the observed process is indeed pseudo first order and

is apparently free from secondary reactions. However, linearity of such plots is not always a good indication of a system free of significant complications as was found in a recent study of some $Cl(^2P)$ + alkane reactions.[17] A consistent feature of such plots is the small positive intercept on the ln ([OH]/[OH]*) axis. The value of the intercept appears to be dependent upon $[O]_0$ and, for a given value of $[O]_0$, dependent upon total flow. It can be seen from eq III that, when the magnitude of k_2' is not infinite compared to k_1', curvature would be expected at short reaction times, such that extrapolation of the linear portion of the plot would result in a negative intercept on the ln ([OH]/[OH]*) axis. However this feature is predicted to be quite small with the experimental conditions used in this study (typically < −0.04) and in contrast to the positive intercept that was actually observed. The positive intercept shown in Figure 3 can possibly be explained in four ways: (a) the reaction of $O(^3P)$ with the phosphoric acid coating to produce OH, i.e., $O + H_3PO_4 \rightarrow OH$ + phosphate product; (b) efficient quenching of the $A^2\Sigma^+$ state of OH by $O(^3P)$ in the resonance-fluorescence region, (c) an uncertainty in the origin of the time axis, or (d) an extra production of OH when O atoms are not present, thus increasing $[OH]_t$ but not $[OH]_t$*. The first explanation is thought to be quite unlikely except possibly at higher temperatures ($T > 500$ K) where it was observed that the OH fluorescence signal actually increased upon addition of $O(^3P)$ to the flow system. The second explanation is entirely consistent with the observations but would require a quenching rate constant for the process

$$OH(^2\Sigma^+) + O(^3P) \rightarrow OH(^2\Pi) + O(^3P) \qquad (5)$$

of greater than 10^{-8} cm^3 molecule^{-1} s^{-1}, which is unacceptably high (this assumes that the reactivity of the $^2\Sigma^+$ state is not ~1000 times greater than the $^2\Pi$ state). There have been numerous studies of the quenching rates for the $A^2\Sigma^+(v = 0)$ state of OH with several different molecules including N_2,[22] H_2O,[22] O_2,[22] and a series of halogenated alkanes.[23] The most efficient quenching gases include H_2O and CCl_4 with values reported for their quenching rate constants, k_q, of $(5 \pm 2) \times 10^{-10}$ cm^3 molecule^{-1} s^{-1} (ref 22) and 1.0×10^{-9} cm^3 molecule^{-1} s^{-1} (ref 23), respectively. The third explanation cannot be ruled out because of the design of the fluorescence cell, but no comparable intercepts were observed in a previous study of Cl + RH reactions using a similar cell design.[17] However, it should be noted that, if either explanation b or c is the reason for the intercept, and explanation a is thought to be highly unlikely, then the value of k_1' which is derived from the slope of plots such as those shown in Figure 3 does not require knowledge of the intercept. Explanation d will be discussed in more detail later.

The values of −d ln ($[OH]_t/[OH]_t$*)/dt were corrected for axial diffusion by using the following equation:[24]

$$k = k'(1 + (k' + 2k_w)D/v^2)$$

where k = corrected first-order rate constant, k' = observed first-order rate constant, k_w = first-order rate contant for heterogeneous loss, v = flow-tube velocity, and D = diffusion coefficient for OH radicals in helium. The diffusion coefficient for OH in He was taken to be $1.08 \times D$(He–Ne), where the factor of 1.08 equals the ratio of the square roots of the molecular weights of OH and Ne. D(OH–He) was taken to be $2.74 \times 10^{-2}T^{1.509}/(\ln [T/(2.12 \times 10^7)])^2 \cdot \exp(1.87/T)$ atm cm^2 s^{-1}.[25] The correction factors were typically 6% (221 K), 3% (260 K), 9% (298 K), 6% (400 K), and 7% (499 K). No corrections were necessary for radial diffusion, i.e., α ($=D/(kr^2)$) was normally much greater than unity, resulting in minimal radial concentration gradients of OH radicals across the flow tube.[26] Table I summarizes the experimental data obtained in this study. Although the values shown for k' have been corrected for axial diffusion, no corrections were made for removal of $O(^3P)$ by OH (due to low initial stoichiometries) as the correction factor was typically <5%. Figure 4 shows a plot of the pseudo-first-order rate constant, k', vs. atomic-oxygen concentration at 400 K. The slopes (bimolecular rate constant, k_1) and intercepts of such plots are obtained from a least-squares treatment of the data. The bimolecular rate constants and intercepts generated in this manner are shown in Table II. The value obtained for k_1 at 298 K was $(3.1 \pm 0.6) \times 10^{-11}$ cm^3 molecule^{-1} s^{-1}. The kinetic runs performed at 298 K using the N + NO reaction as the source of atomic oxygen are in good agreement with the runs where atomic oxygen was produced from an O_2/He discharge. This suggests that there were no kinetic complications from metastable molecular oxygen, $O_2(^1\Delta_g, ^1\Sigma^+)$, produced in the O_2/He discharge. A consistent feature of every plot of k' as a function of atomic-oxygen concentration at each temperature was the negative intercept on the k' axis. The magnitude was typically −20 s^{-1}. From eq IV it can be seen that a negative intercept can be interpreted as the difference in the first-order heterogeneous rate constant, k_w* − k_w, for OH removal when oxgen atoms are, and are not, present, respectively. As stated earlier, k_w was measured during every kinetic run and was determined to be ~15 s^{-1} independent of temperature. Consequently, a negative intercept of ~−20 s^{-1} is consistent, within experimental uncertainty of reducing the rate constant for heterogenous removal of OH to ~0. Computer simulations of the system (which will be discussed in more detail later) performed with both sets of conditions, i.e., k_w* = k_w and k_w* = 0, confirm this observation.

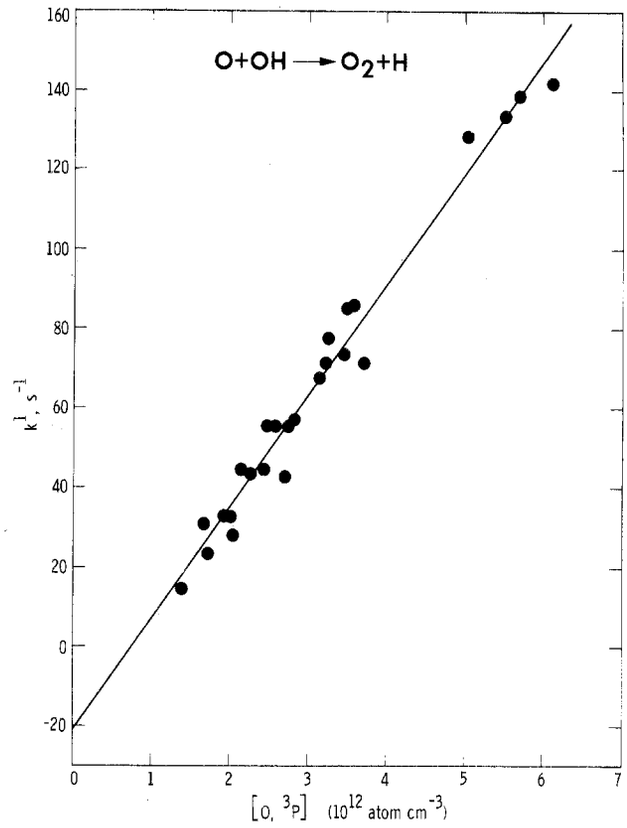

Figure 4. The reaction $O(^3P)$ + OH → O_2 + H. Variation of pseudo-first-order rate constant, −d ln [OH]/dt, with [O,^{3}P] at 408 K.

Potential complications to the kinetic study include (a) removal of $O(^3P)$ by NO_2, (b) removal of OH via the OH

TABLE I: Summary of Experimental Data

temp, K	flow velocity, cm s^{-1}	$[O]_0$, 10^{12} cm^{-3}	$[OH]_0$, 10^{12} cm^{-3}	k', s^{-1}
221	1146	2.11	0.25	51.9
	1192	2.18	0.32	46.7
	1139	2.52	0.32	47.4
	1193	3.07	0.32	54.9
	1143	3.33	0.32	95.0
	1132	4.28	0.33	103
	1140	4.69	0.33	144
	1211	4.75	0.32	137
	1206	6.09	0.32	163
	1135	6.20	0.33	193
	965	6.39	0.42	194
	1139	6.78	0.31	213
	1205	7.32	0.33	174
260	1329	1.26	0.23	25
	1334	1.43	0.12	20.6
	1323	1.54	0.20	17.1
	1334	1.84	0.19	34.2
	1321	2.01	0.23	44.6
	1341	2.29	0.40	51.6
	1350	3.11	0.37	77.6
	1339	3.62	0.12	87.4
	1336	3.94	0.18	96.9
	1342	4.62	0.19	134
298	857	1.73	0.25	52.7
	875	2.23	0.25	65.9
	849	2.56	0.34	55.2
	851	2.89	0.20	73.3
	875	3.04	0.25	66.3
	1103	3.37	0.29	81.6
	1121 (N + NO)	3.39	0.30	120
	884	3.57	0.30	109
	1123 (N + NO)	3.60	0.12	120
	1118	3.65	0.32	117
	1075	3.74	0.31	82.2
	1105	3.91	0.25	126
	1086	4.03	0.26	141
	1099	4.10	0.32	131
	1040 (N + NO)	4.21	0.32	122
	1143	4.27	0.29	117
	1084	4.42	0.32	126
	1139 (N + NO)	4.92	0.15	153
	1121 (N + NO)	4.99	0.29	132
	1137	5.12	0.25	112
	1126 (N + NO)	5.88	0.31	156
408	1365	1.37	0.22	14.3
	982	1.67	0.20	30.2
	944	1.73	0.21	23.1
	1248	1.92	0.27	33.1
	1286	2.01	0.28	32.9
	1936	2.02	0.09	27.9
	1234	2.16	0.15	44.4
	1377	2.25	0.21	43.5
	1253	2.45	0.39	44.6
	1355	2.47	0.23	55.1
	1387	2.52	0.11	55.3
	1962	2.70	0.15	42.4
	996	2.74	0.39	55.9
	1281	2.77	0.32	56.9
	1236	3.15	0.15	68.0
	1276	3.23	0.22	71.3
	1261	3.45	0.29	73.4
	1226	3.50	0.29	85.1
	1401	3.52	0.21	85.5
	1393	3.70	0.27	71.6
	1410	5.02	0.28	129
	1373	5.50	0.27	134
	1357	5.71	0.26	139
	1416	6.16	0.30	142
499	1425	1.95	0.25	21.7
	1472	1.97	0.26	24.2
	1480	2.02	0.28	24.6
	1489	2.24	0.29	36.8
	1485	2.75	0.30	50.4
	1538	3.01	0.30	54.0
	1413	3.22	0.24	58.0
	1458	4.14	0.21	72.6
	1450	5.39	0.21	109
	1438	5.50	0.23	107
	1383	6.21	0.22	123
	1436	6.61	0.24	144

TABLE II: Bimolecular Rate Constants

temp, K	$10^{11}k_1$, cm^3 molecule^{-1} s^{-1}	intercept, s^{-1}
221	3.21 ± 0.28 (3.40)[a]	−(23 ± 14)
260	3.26 ± 0.17 (3.46)	−(25 ± 5)
298	3.10 ± 0.60 (3.35)	−(5 ± 15)
408	2.80 ± 0.10 (3.11)	−(21 ± 3)
499	2.40 ± 0.08 (2.77)	−(21 ± 3)

[a] "Best-fit" values of k_1 are given in parentheses.

+ OH reaction, (c) increased reactivity of OH radicals formed vibrationally excited, and (d) formation of a steady-state concentration of OH by the reaction sequence

$$H + O_2 + M \rightarrow HO_2 + M \quad (6)$$

$$O + HO_2 \rightarrow OH + O_2 \quad (7)$$

$$H + HO_2 \rightarrow 2OH \quad (8)$$

The first three of these potential complications were unimportant because of the experimental conditions used in this study: (a) The ratio of the concentrations of atomic hydrogen to atomic oxygen, $[H]_0/[O]_0$, ranged from 2 to 12 with a typical value of ~5. This ratio, combined with the difference in reactivity of NO_2 with $H(^2S)$ and $O(^3P)$, $k_2/k_4 \approx 15$, means that ~99% of the NO_2 is removed by atomic hydrogen, thus ensuring that a negligible (<1%) concentration of atomic oxygen was removed by NO_2. (b) The low initial concentration of OH radicals, typically ~2 × 10^{11} cm^{-3}, ensured that there was negligible (<0.5%) removal of OH via reaction 9. Typical half-lives due to

$$OH + OH \rightarrow H_2O + O \quad (9)$$

$k_9 = 1.8 \times 10^{-12}$ cm^3 molecule^{-1} s^{-1} (ref 12)

reactions 1 and 9 were ~0.02 (see Table I) and ~4 s, respectively, verifying that reaction 9 is unimportant. Equations I–IV were derived by correctly assuming that reaction 9 could be neglected. (c) The hydroxyl radicals formed in the $H + NO_2$ reaction (eq 2) have been shown to be vibrationally excited with an initial distribution of $OH(v = 0):OH(v = 1):OH(v = 2)$ of 1.4:1.0:0.4.[27] In another study[28] an initial distribution of $OH(v = 1):OH(v = 2):OH(v = 3)$ of 1.0:1.0:0.1 (after correction due to vibrational cascading) was reported. However, this vibrational excitation will have no effect on the determination of k_1 because of the rapid vibrational quenching of OH* due to the large excess concentration of atomic hydrogen always present in this study. Rate constants for the nonreactive quenching of $OH(v = 2)$ and $OH(v = 1)$ by atomic hydrogen (eq 10) were measured to be 3.3×10^{-10} and $2.7 \times$

$$OH(v) + H(^2S) \rightarrow OH(v - 1) + H(^2S) \quad (10)$$

10^{-10} cm^3 molecule^{-1} s^{-1}, respectively.[27] With an atomic-hydrogen concentration of $\sim 1.5 \times 10^{13}$ atoms cm^{-3}, the vibrationally excited hydroxyl radicals will be rapidly deexcited into the ground vibrational level, $\tau_{1/2} \approx 0.5$ ms, i.e., within the mixing region, compared to the time over which reaction 1 was studied, i.e., typically ~30 ms.

TABLE III: Summary of Experimental Values of $k_1(O + OH \rightarrow H + O_2)$

ref		$10^{11}k$, cm^3 molecule^{-1} s^{-1}	temp, K	technique
Del Greco and Kaufman	2	0.6-1.2	310	DF/UV absorption
Clyne	3	5 ± 1.7	265	DF/chemiluminescence
		5 ± 1.7	293	
Kaufman and Del Greco	4	1.8 ± 0.7	310	DF/UV absorption
Kaufman	5	5 ± 2	310	DR/UV absorption/chemiluminescence
Westenberg and De Haas	6	0.5	300	DF/ESR
Breen and Glass	7	4.3 ± 1.3	300	DF/ESR
Westenberg et al.	8	4.1 ± 0.5	228	DR/stirred reactor/ESR
		3.2 ± 0.4	298	
		3.2 ± 0.6	340	
Howard and Smith	9	3.8 ± 0.9	298	DF-FP/RF
Campbell and Handy	13	3.9[b]	425	DF/chemiluminescence
	this study[a]	3.1 ± 0.8	298	DR/RF

[a] Only the 298 K data is included in this table. Table II summarizes all the data obtained in this study. [b] Determined relative to $k(OH + CO)$. $k(OH + CO)$ taken to be 1.5×10^{-13} cm^3 molecule^{-1} s^{-1}.

Consequently there were no complications due to vibrational excitation of OH. (d) Since the oxygen discharge leaves a large fraction of the O_2 undissociated, the formation of HO_2 should occur under our experimental conditions, and reactions 6 and 8 will be the dominant source of OH production. Computer simulation of this effect using reactions 1–2, 6–8, and a wall-loss term indicate that a steady-state concentration of OH should be reached in 150–200 ms, i.e., within the reaction time available with the flow velocities used in this study. An upper limit to this concentration is ~20% of [OH] produced by reaction 2 when O atoms are not present, and a much smaller value in the presence of O atoms. This is believed to be a strong upper limit to this effect, as we observed only a very small (≤10%) correlation between O_2 flow rate and [OH] (t = 0). This results in an increase in the value of $[OH]_t$ used in the kinetic analysis, but not $[OH]_t$*. Three effects stem from this: (1) the decay plots will exhibit a positive intercept which increases with increasing O_2 flow rate (and hence, increasing [O]); (2) the decay plots will show curvature at long reaction times, especially for reactions with high [O] (as has been observed); and (3) the observed value of k_1 will be lower than the "true" value of k_1 by 6–10%, the largest correction being made to the smallest value of k_1 (i.e., at the highest temperatures).

An Arrhenius plot of the bimolecular rate constants shown in Table II is shown in Figure 5. A least-squares fit to the data yields the expression

$$k_1 = (2.01 \pm 0.18) \times 10^{-11} \exp((112 \pm 29)/T)$$

The units used are cm^3 molecule^{-1} s^{-1}, and the activation energy is expressed in units of K^{-1}. An alternate expression which describes k_1 as a function of temperature equally well is

$$k_1 = (2.37^{+1.23}_{-0.81}) \times 10^{-10} T^{-(0.362 \pm 0.072)}$$

The quoted uncertainties are one standard deviation. Because of the limited temperature range and the magnitude of the temperature dependence of k_1, it is not possible to tell whether the Arrhenius or T^{-n} expression would best describe k_1 over a wide range of temperature.

As was stated earlier, the production of a steady-state concentration of OH will lower the observed value of k_1 by ~10% at high temperatures and by ~6% at the lowest temperature used in this study. An iterative procedure was used to find the "best fit" value of k_1 which matched the observed value of k_1. The "best fit" values are also shown in Table II. A least-squares fit to these data yields the expression

$$k_1 = 2.48 \times 10^{-11} \exp(80/T)$$

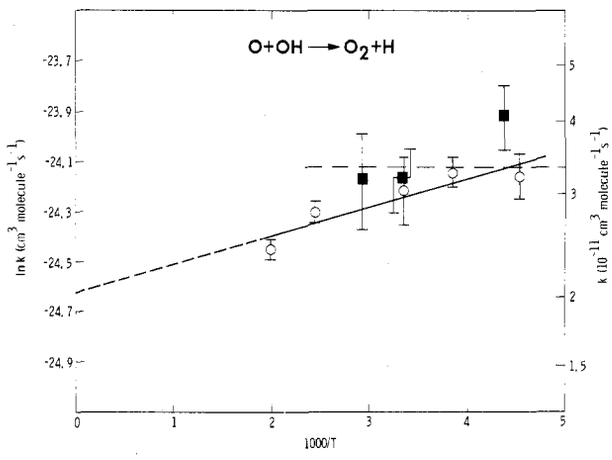

Figure 5. Arrhenius plot for the $O(^3P) + OH \rightarrow O_2 + H$ reaction: (○) this work; (■) ref 8.

Again the units are cm^{-3} molecule^{-1} s^{-1}, and the activation energy is given in K^{-1}. No error limits are given for the "best fit" data as these data are intended only to give another measure of the reliability of the observed data. This does, however, point out that the very small error limits associated with the 408 and 499 K data are clearly fortuitous.

Discussion

Table III summarizes all previous data for the $O(^3P)$ + OH rate constant, k_1, including the unpublished result of Howard and Smith[9] which was communicated to us after completion of our study. The room-temperature value reported in our study is slightly lower than those reported in the earlier less direct kinetic studies[3,5,7,8] and the only other direct kinetic study[9] but is in agreement within the stated uncertainty limits which range from 20 to 40%. The results of the present study and those of Howard and Smith suggest that the value of k_1(298 K) probably lies between 3×10^{-11} and 4×10^{-11} cm^3 molecule^{-1} s^{-1}, in good agreement with the value reported by Westenberg et al.[8] but lower than the other indirect studies. Howard and Smith calculated k_1 to be 3.1×10^{-11} cm^3 molecule^{-1} s^{-1} at 298 K by a method devised by Quack and Troe,[29] which locates the transition state at the configuration of maximum free energy of the reaction coordinate. This value, which is in excellent agreement with that determined in this study, was calculated by assuming that the reaction only proceeds across the X^2A'' surface of HO_2, with the two O atoms being separated by 3.8 Å in the transition state.

The temperature dependence of k_1 measured in this study, while small, does appear to be significant. The only other study which determined k_1 over a reasonable range of temperature was that of Westenberg et al.[8] using a stirred reactor with ESR detection. Although Westenberg et al. reported that the rate constant was invarient with temperature, their actual individual values of k_1 do show some variation with temperature as shown in Figure 5. The values shown are of their data, and the error bars represent one standard deviation. A line drawn through their data, although consistent with no temperature dependence, is also consistent with a temperature dependence of the same magnitude reported in the present study. In addition to the magnitude of the temperature dependence being similar, the absolute values of the rate constants are in good agreement. However, both sets of data, and especially Westenberg et al.'s, are too limited for further comparisons to be made. The value of k_1 at 425 K reported by Campbell and Hardy[13] is not in agreement with the present study within the one-standard-deviation limits.

The negative temperature dependence of k_1 observed in this study is characteristic of a growing number of rapid bimolecular reactions involving atoms and radicals, e.g., $O + ClO$,[30] $O + NO_2$,[31] $NO + ClO$,[30,32] $NO + BrO$,[33,34] $NO + HO_2$,[35,36] and $BrO + BrO$.[37] Several different hypotheses have been proposed to account for this behavior, including a temperature-dependent A factor,[31,34] metastable complex formation,[32,38] and dependence of the collision cross section on reactant energy.[39,40] Alternatively, the observed dependence is small enough to be due to systematic experimental error in several cases.

According to absolute rate theory, the A factor for a bimolecular reaction such as $O(^3P) + OH \rightarrow HO_2^{\ddagger} \rightarrow H + O_2$ is given by

$$A = \frac{kT}{h} \frac{q^{\ddagger}_{HO_2}}{q_O q_{OH}}$$

where $q = q_{elec} q_{vib} q_{rot} q_{trans}$ (composite partition function).[41] When $O(^3P)$ reacts with OH to form a nonlinear $HO_2^{\ddagger}$ activated complex, the product of kT/h and the translational and rotational partition functions is invariant with temperature. The temperature dependence of the vibrational partition function ratio is predominantly controlled by the temperature dependence of the bending mode of $HO_2^{\ddagger}$, which can range from temperature invariant (tight complex where $\bar{\nu} \approx 1390$ cm^{-1})[42] to $\sim T^{0.9}$ (loose complex where $\bar{\nu} \approx 75$ cm^{-1}). Consequently, according to absolute rate theory the A factor should be either temperature invariant or exhibit a small positive temperature dependence. This is consistent with the expression of $k_1 = 10^{16.6} \cdot \exp(\Delta S^{\circ}_{300}{}^{\ddagger}/R) T^{0.5 \pm 0.5}$ derived by Benson et al.[43]

The negative temperature dependence observed in this reaction can be explained by an argument similar to that used by Smith and Zellner[44] and Leu and DeMore[32] in explaining the temperature dependences of the OH + CO and ClO + NO reactions, respectively, by invoking the mechanism

$$O + OH \underset{k_{-1}}{\overset{k_1}{\rightleftharpoons}} (HO_2)^{\ddagger} \xrightarrow{k_2} O_2 + H$$

A vibrationally "hot" HO_2 radical is formed which may decompose to either products or reactants. Steady-state analysis of this mechanism yields an observed rate constant of the form

$$k_{obsd} = \frac{k_1 k_2}{k_{-1} + k_2}$$

The negative temperature dependence of k_{obsd} requires that k_{-1} be more strongly temperature dependent than k_2 and comparable in magnitude. Following the arguments of Leu and DeMore,[32] the RRK theory gives the unimolecular rate expressions for k_{-1} and k_2 in the form

$$k = A\left(\frac{E^* - E_c}{E^*}\right)^{s-1}$$

where E^* is the total excitation energy ($\sim$67 kcal mol^{-1} in this system), E_c is the threshold energy of the reaction, and s is the effective number of oscillators. The quantity $E^* - E_c$ is determined mainly by the exothermicity of the overall reaction for k_2, but mainly by thermal energy for k_{-1} ($\sim$2 kcal mol^{-1}); hence, k_{-1} will be much more temperature dependent than k_2. The ratio k_2/k_{-1} can be written

$$\frac{k_2}{k_{-1}} = \frac{A_2}{A_{-1}}\left(\frac{E^* - E_c(2)}{E^* - E_c(-1)}\right)^{s-1}$$

The range of possible values for s is 1–3, with a most probable value of 2. Consequently $k_2/k_{-1} \simeq 10A_2/A_{-1}$, with the value decreasing with increasing temperature. Therefore for k_{-1} to compete with k_2, the condition $A_{-1} \simeq 10A$ must be met. From transition-state theory the A factors for reactions −1 and 2 can be written as

$$A = \frac{kT}{h} \frac{q^{\ddagger}_{trans} q^{\ddagger}_{rot} q^{\ddagger}_{vib}}{q^{HO_2}_{trans} q^{HO_2}_{rot} q^{HO_2}_{vib}}$$

The translational partition functions will cancel and therefore have no effect. The transition state for the reverse reaction (reaction −1) will stretch the O–O bond to $\sim$3.7 Å (2.8 times the normal O–O bond length, in agreement with the estimate of Howard and Smith[9] of the O–O bond length at the point of maximum free energy), which results in a rotational partition function ratio, $q^{\ddagger}_{rot}/q^{HO_2}_{rot}$ of $\sim$10, whereas a similar calculation for the transition state of the forward reaction (reaction 2) yields a ratio of $\sim$2 for $q^{\ddagger}_{rot}/q^{HO_2}_{rot}$ when the O–H bond is stretched to $\sim$2.7 Å. An analysis of the vibrational partition functions indicates that the O–O–H bending mode is the major contributor to their values. If the bending mode is treated as a hindered free rotation in the transition state, Benson's methods[45] can be applied to calculate the entropy of such a rotor, and from this the frequency of the vibrations required to give the equivalent entropy. Values of $\sim$75 and $\sim$500 cm^{-1} are estimated for reactions −1 and 2, respectively. This will contribute a factor of 2.5–4 (for the temperature range 220–500 K) to the ratio k_{-1}/k_2.

From this approximate treatment we can therefore demonstrate that the A factor ratio A_{-1}/A_2 is in the range $\sim$10–20 for the temperatures used in the present study. Combining this A factor ratio with the $E^* - E_c$ ratio results in a value of 1–2 for k_{-1}/k_2. In light of these arguments, the proposed explanation of the temperature dependence seems quite plausible.

It must be pointed out that this argument depends strongly on the special circumstances of this reaction, i.e., the ejection of a light atom as the "product channel". We feel, however, that a mechanism of this type is probably common to all of the aforementioned reactions[30-37] and that this kinetic argument or one based on this mechanism can be made for all of these systems.

It can also be argued that the temperature dependence of the reaction is due to the temperature dependence of the $O(^3P)$ and OH electronic partition functions. This may be true for many of the aforementioned reactions, but again we feel that the more unifying approach of a kinetic

TABLE IV

temp, K	$\Delta H°$, kcal mol^{-1}	$\Delta S°$, cal K^{-1} mol^{-1}	K_p	k_1(calcd)[af]	k_1(calcd)[bf]	k_1(exptl)[cf]	k_1(exptl)[df]
298	−16.86	−5.96	1.15 (11)	2.07	2.59	2.93	3.01
500	−16.87	−6.01	1.15 (6)	1.95	1.86	2.53	2.50
1000	−16.50	−5.53	2.51 (2)	1.98	1.55	2.26[e]	1.94[e]
1500	−16.02	−5.14	16.3	2.16	1.58	2.17[e]	1.69[e]

[a] $k_{-1} = 3.7 \times 10^{-10} \exp(-8450/T)$ cm^3 molecule^{-1} s^{-1} (ref 15). [b] $k_{-1} = 2.37 \times 10^{-10} \exp(-8250/T)$ cm^3 molecule s^{-1} (ref 16). [c] $k_1 = 2.01 \times 10^{-11} \exp(112/T)$ cm^3 molecule^{-1} s^{-1}. [d] $k_1 = 2.37 \times 10^{-10}\ T^{-0.362}$ cm^3 molecule^{-1} s^{-1}. [e] These values were derived by extrapolating the expressions for k_1 outside the experimental temperature range. [f] In units of 10^{11} cm^3 molecule^{-1} s^{-1}.

argument is more appropriate for this class of reactions.

As stated in the introduction there is a discrepancy of a factor of ~2 between the equilibrium constant, $K_{eq} = k_1/k_{-1}$, determined by using thermodynamic data and that using the experimental values of k_1 and k_{-1} when the value of k_1 is taken to be $\sim 4 \times 10^{-11}$ cm^3 molecule^{-1} s^{-1} and to be invariant with temperature.[10-12] Using the preferred[46] thermodynamic values of $\Delta H°_{298}$, $S°_{298}$, and C_p, for O(^{3}P), H(^{2}S), OH($^2\Pi$), and O$_2$($^3\Sigma_g^-$) the equilibrium constants shown in Table IV can be derived. Two of the evaluated expressions[15,16] for the temperature dependence of k_{-1} are combined with the calculated equilibrium constants (thermodynamic) to yield values for k_1 at 298, 500, 1000, and 1500 K. These calculated values of k_1 and the values of k_1 that can be derived from the Arrhenius and T^{-n} expressions which were determined in the present study are shown in Table IV. It can be seem that combining the thermodynamic equilibrium constant with the Baulch et al.[15] value of k_{-1} results in a value of $\sim 2 \times 10^{-11}$ cm^3 molecule^{-1} s^{-1} which is nearly independent of temperature. In contrast, combining the thermodynamic equilibrium constant with the Dixon-Lewis and Williams[16] value for k_{-1} results in values of k_1 decreasing from 2.59×10^{-11} to 1.58×10^{-11} cm^3 molecule^{-1} s^{-1} as the temperature increases from 298 to 1500 K. The values of k_1 derived from the experimental expressions range from 2.93×10^{-11} to 2.17×10^{-11} cm^3 molecule^{-1} s^{-1} and 3.01×10^{-11} to 1.69×10^{-11} cm^3 molecule^{-1} s^{-1} as the temperature increases from 298 to 1500 K. Consequently, while the agreement between the calculated and extrapolated experimental values of k_1 is good at the two highest temperatures, 1000 and 1500 K, the agreement is less satisfactory at 298 and 500 K. This could easily be explained by a nonlinearity in the Arrhenius behavior of k_{-1}. The experimental data for k_{-1} between 700 and 2500 K is scattered and does not rule out such a nonlinearity. As stated earlier, our experimental data are fitted equally well by either the Arrhenius or T^{-n} expression. Each of these expressions is more compatible with the thermodynamic value of K_{eq} and the experimental values of k_{-1} than the previous data where k_1 was thought to exhibit no temperature dependence with a value of $\sim 4 \times 10^{-11}$ cm^3 molecule^{-1} s^{-1}.

The lower value of k_1 obtained in this study will have some effect on models of HO_x in the upper stratosphere and mesosphere. It can be shown[1] that, at the stratospause level, the ratio [OH]/[HO$_2$] is controlled by the O(^{3}P) + OH (eq 1) and O(^{3}P) + HO$_2$ (eq 11) reactions:

$$O(^3P) + HO_2 \rightarrow OH + O_2 \qquad (11)$$

$$k_{11} = 3.1 \times 10^{-11} \text{ cm}^3 \text{ molecule}^{-1} \text{ s}^{-1} \text{ (ref 12)}$$

Therefore

$$[OH]/[HO_2] = k_{11}/k_1$$

Mesospheric temperatures range from ~275 (stratopause) to ~190 K (~80 km). Consequently the values of k_1 derived from the present study range from 3.0×10^{-11} (stratopause) to 3.6×10^{-11} cm^3 molecule^{-1} s^{-1} (80 km) in contrast to the value of $\sim 4 \times 10^{-11}$ cm^3 molecule^{-1} s^{-1} presently used in the photochemical models. Consequently, using the values of k_1 determined in the present study in the photochemical models, instead of 4×10^{-11} cm^3 molecule^{-1} s^{-1}, would result in predictions of higher [OH]/[HO$_2$] by a factor of 1.1–1.35. Both absolute and relative OH and HO$_2$ concentrations are controlled by reactions whose rate constants are poorly known; e.g., the OH + HO$_2$ reaction (eq 12) controls the absolute concentrations of OH and HO$_2$ by acting as a radical termination reaction. The only study of reaction 11 was by Burrows et al.,[47] who measured O + HO$_2$ (reaction 11) relative to both O + OH (reaction 1) and OH + H$_2$O$_2$ (reaction 13).

$$OH + HO_2 \rightarrow H_2O + O_2 \qquad (12)$$

$$k_{12} = 3.5 \times 10^{-11} \text{ cm}^3 \text{ molecule}^{-1} \text{ s}^{-1} \text{ (ref 12)}$$

$$OH + H_2O_2 \rightarrow H_2O + HO_2 \qquad (13)$$

$$k_{13} = 2.51 \times 10^{-12} \exp(-126/T) \text{ (ref 47)}$$

Burrows et al.[47] reported values of 0.83 and 37 for k_{11}/k_1 and k_{11}/k_{13} at 298 K, respectively. These values were combined with values of 3.8×10^{-11} cm^3 molecule^{-1} s^{-1} for k_1 and 8.3×10^{-12} cm^3 molecule^{-1} s^{-1} for k_{13} to yield values of 3.2×10^{-11} and 3.1×10^{-11} cm^3 molecule^{-1} s^{-1} for k_{11}. However, since the study of Burrows et al., there has been a study of reaction 13 by Keyser[48] (value shown above) which resulted in a value of 1.6×10^{-13} cm^3 molecule^{-1} s^{-1} at 298 K. Consequently, combining Burrows et al.'s values of k_{11}/k_1 and k_{11}/k_{13} with our value of k_1 and Keyser's value of k_{13} yields values of 2.57×10^{-11} and 5.92×10^{-11} cm^3 molecule^{-1} s^{-1} for k_{11}. Obviously, there appears to be some uncertainty in k_{11} which results in an uncertainty in the [OH]/[HO$_2$] concentrations.

Acknowledgment. We thank W. B. DeMore and S. P. Sander for valuable discussions in the course of this work. We also thank one of the referees for an enlightening review of our arguments. The research described in this paper was carried out at the Jet Propulsion Laboratory, California Institute of Technology, under NASA Contract NAS7-100.

References and Notes

(1) Nicolet, M. J. *Geophys. Space Phys.* **1975**, *13*, 593.
(2) Del Greco, F. P.; Kaufman, F., *Discuss. Faraday Soc.* **1962**, *33*, 128.
(3) Clyne, M. A. A. *Symp. (Int.) Combust., [Proc.]* **1963**, *9*, 211.
(4) Kaufman, F.; Del Greco, F. P. *Symp. (Int.) Combust., [Proc.]* **1963**, *9*, 659.
(5) Kaufman, F. *Ann. Geophys.* **1964**, *20*, 106.
(6) Westenberg, A. A.; de Haas, N. *J. Chem. Phys.* **1965**, *43*, 1550.
(7) Breen, J. G.; Glass, G. P. *J. Chem. Phys.* **1970**, *52*, 1082.
(8) Westenberg, A. A.; de Haas, N.; Roscoe, J. M. *J. Phys. Chem.* **1970**, *74*, 3431.
(9) Howard, M. J.; Smith, I. W. M. *Chem. Phys. Lett.* **1980**, *69*, 40.
(10) Hampson, R. F., Jr., and Garvin, D., Eds. *Natl. Bur. Stand. (U.S.), Spec. Publ.* **1978**, 513.
(11) DeMore, W. B.; Stief, L. J.; Kaufman, F.; Golden, D. M.; Hampson, R. F., Jr.; Kurylo, M. J.; Margitan, J. J.; Molina, M. J.; Watson, R. T.

"Chemical Kinetic and Photochemical Data for use in Stratospheric Modelling"; Evaluation No. 2, NASA Panel for Data Evaluation 1979, JPL Publication 79-27.
(12) Baulch, D. L.; Cox, R. A.; Hampson, R. F., Jr.; Kerr, J. A.; Troe, J.; Watson, R. T. "Evaluated Kinetic and Photochemical Data for Atmospheric Chemistry"; CODATA Task Group on Chemical Kinetics, 1979, CODATA Bulletin No. 33 and *J. Phys. Chem. Ref. Data* **1980**, *9*, 295.
(13) Campbell, I. M.; Handy, J. *Chem. Phys. Lett.* **1977**, *47*, 475.
(14) See references listed in ref 15, pp 9–36.
(15) Baulch, D. L.; Drysdale, D. D.; Horne, D. G.; Lloyd, A. C. "Evaluated Kinetic Data for High Temperature Reactions"; Butterworths: London, 1972; Vol. 1. This review discusses previous evaluations.
(16) Dixon-Lewis, G.; Williams, D. J. *Compr. Chem. Kinet.* **1977**, *17*, Chapter 1.
(17) Lewis, R. S.; Sander, S. P.; Wagner, S. G.; Watson, R. T. *J. Phys. Chem.* **1980**, *84*, 2009.
(18) Michael, J. V.; Nava, D. F.; Payne, W. A.; Lee, J. H.; Stief, L. J. *J. Phys. Chem.* **1979**, *83*, 2818. The 298 K value is in excellent agreement with those reported by the following: Wagner, H. Gg.; Welzbacher, U.; and Zellner, R. *Ber. Bunsenges. Phys. Chem.* **1976**, *80*, 1023. Clyne, M. A. A.; Monkhouse, P. B. *J. Chem. Soc., Faraday Trans. 2* **1977**, *73*, 298. Bemand, P. P.; Clyne, M. A. A. Ibid. **1977**, *73*, 394. However, there is a discrepancy in the reported values for the activation energy. The value quoted in this paper is that of Michael et al.; however, our determination of k_1(O + OH → O_2 + H) is not sensitive to the value used.
(19) Wiese, W. L.; Smith, M. W.; Glennon, B. M. *Natl. Stand. Ref. Data Ser. (U.S., Natl. Bur. Stand.)* **1969**, *No. 1*.
(20) Clyne, M. A. A.; Cruse, H. W. *J. Chem. Soc., Faraday Trans. 2* **1972**, *68*, 1281.
(21) Kaufman, F. *Prog. React. Kinet.* **1961**, *1*, 2. See references contained within this review.
(22) Selzer, P. M.; Wang, C. C. *J. Chem. Phys.* **1979**, *71*, 3786. See this reference and some of the references cited therein .
(23) Clyne, M. A. A.; Holt, P. M. *J. Chem. Soc., Faraday Trans. 2* **1979**, *75*, 569.
(24) Howard, C. J. *J. Phys. Chem.* **1979**, *83*, 3.
(25) Marrero, T. R.; Mason, E. A. *J. Phys. Chem.* Ref. *Data* **1972**, *1*, 3.
(26) Poirier, R. V.; Carr, R. W., Jr. *J. Phys. Chem.* **1971**, *75*, 1593.
(27) Spencer, J. E.; Glass, G. P. *Chem. Phys.* **1976**, *15*, 35.
(28) Polanyi, J. C.; Sloan, J. J. *Int. J. Chem. Kinet. Symp.* **1975**, *1*, 51.
(29) Quack, M.; Troe, J. *Ber. Bunsenges. Phys. Chem.* **1977**, *81*, 329.
(30) Zahniser, M. S.; Kaufman, F. *J. Chem. Phys.* **1977**, *66*, 3673.
(31) Bemand, P. B.; Clyne, M. A. A.; Watson, R. T. *J. Chem. Soc., Faraday Trans. 2* **1974**, *70*, 564.
(32) Leu, M. T.; DeMore, W. B. *J. Phys. Chem.* **1978**, *82*, 2049.
(33) Leu, M. T. *Chem. Phys. Lett.* **1979**, *61*, 275.
(34) Watson, R. T.; Sander, S. P.; Yung, Y. L. *J. Phys. Chem.* **1979**, *83*, 2936.
(35) Leu, M. T. *J. Chem. Phys.* **1979**, *70*, 1662.
(36) Howard, C. J. *J. Chem. Phys.* **1979**, *71*, 2352.
(37) Sander, S. P.; Watson, R. T., submitted to *J. Phys. Chem.*
(38) Singleton, D. L.; Cvetanovic, R. J. *J. Am. Chem. Soc.* **1976**, *98*, 6812.
(39) Davis, D. D.; Hule, R. E.; Herron, J. T. *J. Chem. Phys.* **1973**, *59*, 628.
(40) Jaffe, R. L. "Can A Bimolecular Gas Phase Reaction Have A Negative Activation Energy?", presented at the 175th National Meeting of the American Chemical Society, Anaheim, CA, 1978.
(41) Laidler, K. J. "Chemical Kinetics", 2nd ed.; McGraw-Hill: New York, 1965; Chapter 3.
(42) Paukert, T. T.; Johnston, H. S. *J. Chem. Phys.* **1972**, *56*, 2824.
(43) Benson, S. W.; Golden, D. M.; Lawrence, R. W.; Shaw, R.; Woolfolk, R. W. *Int. J. Chem. Kinet., Symp.* **1975**, *1*, 399.
(44) Smith, I. W. M.; Zellner, R. *J. Chem. Soc., Faraday Trans. 2*, **1973**, *69*, 1617.
(45) Benson, S. W. "Thermochemical Kinetics", 2nd ed.; Wiley: New York, 1976.
(46) The thermodynamic values were taken from the following sources: ref 13 for all values of ΔH°_{298} and S°_{298} except ΔH°_{298}(OH) which was taken as 9.41 kcal mol^{-1}, not 9.31 kcal mol^{-1} (D. Wagman, National Bureau of Standards, Washington, D.C., private communication. Wagman's evaluation of ΔH°_0(OH) agrees with the JANAF value of 9.31 kcal mol^{-1}, but disagrees with the JANAF value of 9.47 kcal mol^{-1} for ΔH°_{298}(OH)). C_p values were taken from ref 45.
(47) Burrows, J. P.; Cliff, D. I.; Harris, G. W.; Thrush, B. A.; Wilkinson, J. P. T. *Proc. R. Soc. London* **1979**, *A368*, 463.
(48) Keyser, L. *J. Phys. Chem.* **1980**, *84*, 1659.

Percolation Transition in Water in Oil Microemulsions. Electrical Conductivity Measurements

M. Laguës and C. Sauterey

Collège de France, Laboratoire de Physique de la Matiere Condensee, 75231 Paris, Cedex 05, France *(Received: March 3, 1980; In Final Form: July 29, 1980)*

We measured the low-frequency (600 Hz) electrical conductivity of water in oil microemulsions composed of water, cyclohexane, SDS, and 1-pentanol. The structure of these microemulsions was previously described in the low water concentration range (water concentration $\sim 10^{-2}$) as a suspension of minute droplets (diameter ~ 100 Å) with weak mutual interaction.[1] Neutron scattering measurements show that the structure of droplets remains unchanged up to a water concentration of, for instance, 0.30.[2] At low water concentration, the electrical conductivity is due to the mean charge of the droplets. The electrical conductivity increases steeply over five orders of magnitude when the concentration of droplets increases. We describe this variation by a percolation transition: beyond a critical volume concentration of droplets, an infinite path exists through aggregated droplets. The critical exponents of the transition depart from theoretical predictions for a solid suspension of conductive particles in an insulating medium. This is explained by the Brownian motion of the droplets. We present a "stirred percolation" model which accounts for the observed critical exponents. A second transition is observed at high water concentration: the microemulsion is inverted from water in oil to oil in water. The effect of both additional alcohol and ionic strength of water are discussed.

I. Introduction

Microemulsions are transparent and fluid systems composed of water, oil, and amphiphilic molecules. If an ionic surfactant is used, a fourth component, and cosurfactant, is needed. The system described in this paper is composed of cyclohexane, water, sodium dodecyl sulfate as surfactant, and 1-pentanol as cosurfactant.

In a previous paper,[1] the structure of this system was described in the low water concentration range (0.005–0.04). Both hydrodynamical and neutron scattering measurements show clearly that water is dispersed in minute droplets of some tens of angströms in diameter.

0022-3654/80/2084-3503$01.00/0